Journal Pre-proof

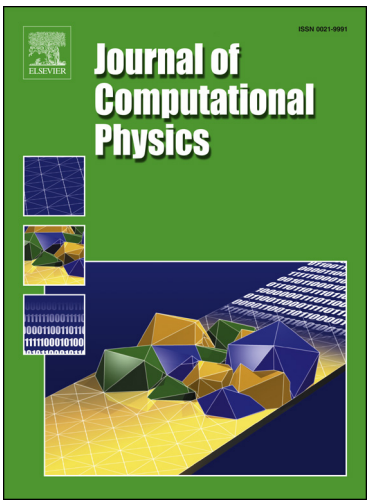

Fast upwind and Eulerian-Lagrangian control volume schemes for time-dependent directional space-fractional advection-dispersion equations

Ning Du, Xu Guo, Hong Wang

PII: S0021-9991(19)30832-0
DOI: https://doi.org/10.1016/j.jcp.2019.109127
Reference: YJCPH 109127

To appear in: *Journal of Computational Physics*

Received date: 6 July 2019
Revised date: 10 October 2019
Accepted date: 11 November 2019

Please cite this article as: N. Du et al., Fast upwind and Eulerian-Lagrangian control volume schemes for time-dependent directional space-fractional advection-dispersion equations, *J. Comput. Phys.* (2019), 109127, doi: https://doi.org/10.1016/j.jcp.2019.109127.

Highlights

- We consider a multidimensional time-dependent space-fractional advection-diffusion equation to model solute transport in heterogeneous porous media and related applications. The equation involves all directions in its fractional derivative rather than only x and y directions.
- We derive the fast control-volume schemes combined with upwind or Eulerian-Lagrangian methods to solve the target FPDE. These schemes naturally have second order accuracy in space without referring to any artificial shift in the numerical discretization and conserve mass locally that is crucial in these applications.
- A fast Krylov subspace iterative solver for both the upwind and Eulerian-Lagrangian control volume schemes is proposed. Numerical experiments show the utility of the method.

Fast upwind and Eulerian-Lagrangian control volume schemes for time-dependent directional space-fractional advection-dispersion equations

Ning Du[a], Xu Guo[b,c,*], Hong Wang[d,*]

[a]*School of Mathematics, Shandong University, Jinan, Shandong 250100, China*
[b]*Geotechnical and Structural Engineering Research Center, Shandong University, Jinan, Shandong 250100, China*
[c]*Department of Mathematics, The Chinese University of Hong Kong, Shatin, N. T., Hong Kong*
[d]*Department of Mathematics, University of South Carolina, SC, 29208, USA*

Abstract

We develop control volume methods for two-dimensional time-dependent advection-dominated directional space-fractional advection-dispersion equations with the directional space-fractional derivative weighted in all the directions by a probability measure in the unit circle, which are used to model the anisotropic superdiffusive transport of solutes in groundwater moving through subsurface heterogeneous porous media.

We develop a fast upwind control volume method for the governing equation to eliminate the spurious numerical oscillations that often occur in space-centered numerical discretizations of advection term, which are relatively straightforward to implement. We also develop a Eulerian-Lagrangian control-volume method for the governing equation, which symmetrizes the governing equation by combining the time-derivative term and the advection term into a material derivative term along characteristic curves. Both methods are locally mass-conservative, which are essential in these applications.

Due to the nonlocal nature of the directional space-fractional differential operators, corresponding numerical discretizations usually generate full stiffness matrices. Conventional direct solvers tend to require $O(N^2)$ mem-

*Corresponding author
Email addresses: duning@sdu.edu.cn (Ning Du), guoxu1014@163.com (Xu Guo), hwang@math.sc.edu (Hong Wang)

ory requirement and have $O(N^3)$ computational complexity per time step, where N is the number of spatial unknowns, which is computationally significantly more expensive than the numerical approximations of integer-order advection-diffusion equations. Based on the analysis of the structure of stiffness matrix, we propose a fast Krylov subspace iterative solver to accelerate the numerical approximations of both the upwind and Eulerian-Lagrangian control volume methods, which reduce computational complexity from $O(N^3)$ by a direct solver to $O(N \log N)$ per Krylov subspace iteration per time step and a memory requirement from $O(N^2)$ to $O(N)$. Numerical results are presented to show the utility of the methods.

Keywords: directional space-fractional advection-dispersion equation, superdiffusive solute transport, Krylov subspace iterative solver, control volume method
2010 MSC: 35R11, 60J60, 65F10, 65F30, 65M06, 65T50

1. Introduction

Traditional second-order time-dependent advection-dispersion equations (ADEs) were derived under the assumptions that underlying particle movements have (i) a mean free path and (ii) a mean waiting time [3, 19]. However, these assumptions hold only for diffusive transport in homogeneous porous media, when solute plumes are observed to have Gaussian type symmetric and exponentially decaying tails [2]. However, field tests showed that solute transport in heterogeneous porous media often exhibits highly skewed and power-law decaying tails, and so cannot be described accurately by integer-order ADEs [3]. Fractional advection-dispersion (FADEs) were constructed so that their solutions are characterized by highly skewed and power-law decaying tails, and so can accurately model the anisotropic superdiffusive transport of solutes in heterogeneous porous media [3, 18, 19, 33].

Nevertheless, numerical discretizations of space-fractional partial differential equations generate dense or full stiffness matrices [7, 8, 15, 16, 17, 18, 20], for which direct solvers require $O(N^2)$ memory and $O(N^3)$ computational complexity per time step that represents significantly increased memory requirement and computational complexity than numerical methods for integer-order ADEs do, especially in multiple space dimensions. It was proved in [29] that the Meerschaert-Tadjeran finite difference method

for one-dimensional space-fractional diffusion equation has a Toeplitz like structure, based on which a Krylov subspace iterative method was developed that reduces significantly the memory requirement from $O(N^2)$ to $O(N)$ and computational complexity from $O(N^3)$ to $O(N \log N)$ per Krylov subspace iteration per time step. It was then proved in [23, 25] that the stiffness matrices of finite difference methods for multi-dimensional space-fractional diffusion equations in coordinate forms have a block-Toeplitz-circulant-block like structure utilizing the tensor-product structure of the stiffness matrices, and corresponding fast solvers were developed. It was proved subsequently in [6] that the stiffness matrix of a finite element method for two-dimensional directional space-fractional diffusion equations in which the directional space-fractional derivative is weighted in all the directions by a probability measure in the unit circle, in which the stiffness matrix of a finite element method was proved to have a block-Toeplitz-Toeplitz-block (BTTB) structure by utilizing the tranlation-invariance property of the numerical scheme. Related fast solution methods also include [13], [31], and [32].

In this paper we consider the time-dependent directional space-fractional advection-dispersion equations in two space dimensions [8, 18, 33]

$$\begin{aligned} &\frac{\partial u}{\partial t} + \nabla \cdot (\vec{v} u) - \int_0^{2\pi} \big(D_\theta \; K \; I_\theta^\beta D_\theta u\big) P(d\theta) = f, \quad (x, y, t) \in \Omega \times (0, T], \\ &\qquad u(x, y, 0) = u_0(x, y), \quad (x, y) \in \Omega. \end{aligned} \tag{1}$$

Here Ω is a rectangular domain in $\mathbb{R}^2$ that is assumed to be the unit square $(0, 1)^2$ for simplicity of notations, $\vec{v} = (v_x, v_y)^T$ is the fluid velocity, $\nabla = (\frac{\partial}{\partial x}, \frac{\partial}{\partial y})^T$, f is the source and sink term, K is a positive diffusivity coefficient, $P(d\theta)$ is a probability measure on $[0, 2\pi)$, D_θ is the differential operator in the direction of $\vec{d}_\theta := (\cos\theta, \sin\theta)^T$

$$D_\theta u := \vec{d}_\theta \cdot \nabla u = \frac{\partial u}{\partial x} \cos\theta + \frac{\partial u}{\partial y} \sin\theta, \tag{2}$$

I_θ^β is the βth order fractional integral operator in the direction of $\vec{d}_\theta$ [8]

$$I_\theta^\beta u(x, y, t) := \int_0^{\gamma_b(\theta; x, y)} \frac{\gamma^{\beta-1}}{\Gamma(\beta)} u(x - \gamma\cos\theta, y - \gamma\sin\theta, t) d\gamma, \quad 0 < \beta < 1 \tag{3}$$

where $\gamma_b(\theta; x, y)$ refers to the instant that the ray emanating from (x, y) in the direction of $-\vec{d}_\theta$ encounters the boundary $\partial\Omega$.

We may close problem (1) by the homogeneous Dirichlet boundary condition or an Ω-periodical boundary condition. These types of boundary conditions often arise in such applications as miscible displacement or solute transport in subsurface porous medium fluid flow problems [1, 2, 9, 11, 26, 27, 28].

Problem (1) is used to model such applications as the anisotropic superdiffusive transport of solutes in groundwater moving through subsurface heterogeneous porous media, in which the probability measure $P(d\theta)$ describes the preferential flow directions in the porous media. In these applications local mass conservation is of fundamental importance, as even very little mass error of toxic solutes may have severe consequences. Therefore, an accurate and mass conservative approximation to problem (1) is desired [2, 9], which motivates the development of control volume methods for problem (1).

Due to the hyperbolic nature of problem (1), the traditional space-centered discretizations to the advection term tend to generate numerical solutions with spurious oscillations unless the mesh Peclet number is impractically small [11, 14, 21, 24, 26]. We develop an upwind control volume method in which the arithmetic mean of the advective fluxes at both cell interfaces in each coordinate direction is replaced by a one-sided cell interface flux depending on the sign of the component of the velocity field at the cell. The method generates stable numerical approximations to problem (1) independent of the size of the mesh Peclet number, and is straightforward to implement.

We also develop a Eulerian-Lagranrian control volume method, in which we combine the time derivative term and the advection term to formulate a material derivative and discretize this term in the Lagrangian coordinate but discretize the directional space-fractional dispersion term on the fixed spatial mesh. This method symmetrizes the FADE in (1) and stabilizes its numerical approximations [1, 5, 10, 14, 22, 24, 26, 27, 28]. It generates accurate numerical solutions and significantly reduces the numerical diffusion and grid-orientation effect present in many Eulerian methods even if large time steps and coarse spatial meshes are used, and is very competitive in terms of accuracy and efficiency [30]. Consequently, the method significantly reduces the size of the discrete linear algebraic systems and the number of time steps.

Finally, because of the nonlocal nature of the directional space-fractional differential operators, corresponding numerical discretizations generate full stiffness matrices. Conventional direct solvers require $O(N^2)$ memory requirement and have $O(N^3)$ computational complexity per time step, which is computationally significantly more expensive than the numerical discretiza-

tions of integer-order advection-diffusion equations. Based on the analysis of the structure of stiffness matrix, we propose a fast Krylov subspace iterative solver to accelerate the numerical simulations of both the upwind and Eulerian-Lagrangian control volume methods, which reduces computational complexity from $O(N^3)$ by a direct solver to $O(N \log N)$ per Krylov subspace iteration per time step and a memory requirement from $O(N^2)$ to $O(N)$.

The rest of the present paper is organized as follows. In Sections 2 and 3 we derive an upwind control volume scheme and a Eulerian-Lagrangian control volume scheme, respectively. In Section 5 we explore the translation invariance properties of fractional directional derivatives and study the structure of the stiffness matrices. In Section 6 we develop a fast Krylov subspace iterative solver for both the upwind and Eulerian-Lagrangian control volume schemes, based on the structure of the stiffness matrix. Several numerical experiments are carried out to investigate the performance of the proposed methods in Section 7. Some concluding remarks are given in the last section.

2. An upwind control-volume scheme

Let N_x, N_y, and N_t be positive integers. We define a uniform temporal partition on $[0,T]$ by $t_k := k\Delta t$ for $k = 0, 1, \ldots, N_t$ with $\Delta t := T/N_t$, and a uniform spatial partition $x_i := ih_x$ and $y_j := jh_y$ for $i = 0, 1, \cdots, N_x+1$ and $j = 0, 1, \cdots, N_y+1$ on $\overline{\Omega}$ with $h_x := 1/(N_x+1)$ and $h_y := 1/(N_y+1)$. Let $x_{i-\frac{1}{2}} := (x_{i-1}+x_i)/2$ and $y_{j-\frac{1}{2}} := (y_{j-1}+y_j)/2$ for $i = 1, 2, \cdots, N_x+1$ and $j = 1, 2, \cdots, N_y+1$, and

$$\Omega_{i,j} := (x_{i-1}, x_{i+1}) \times (y_{j-1}, y_{j+1}), \quad \hat{\Omega}_{i,j} := (x_{i-\frac{1}{2}}, x_{i+\frac{1}{2}}) \times (y_{j-\frac{1}{2}}, y_{j+\frac{1}{2}}). \quad (4)$$

We integrate the governing equation (1) on $\hat{\Omega}_{i,j} \times [t_{k-1}, t_k]$ to obtain

$$\begin{aligned} &\int_{t_{k-1}}^{t_k} \int_{\hat{\Omega}_{i,j}} \Big[\frac{\partial u}{\partial t} + \nabla \cdot (\vec{v}u) - \int_0^{2\pi} \big(D_\theta \; K \; I_\theta^\beta D_\theta u \big) P(d\theta) \Big] dxdydt \\ &\quad = \int_{t_{k-1}}^{t_k} \int_{\hat{\Omega}_{i,j}} f(x,y,t) dxdydt. \end{aligned} \quad (5)$$

We evaluate the first term on the left-hand side by

$$\int_{t_{k-1}}^{t_k} \int_{\hat{\Omega}_{i,j}} \frac{\partial u}{\partial t} dxdydt = \int_{\hat{\Omega}_{i,j}} u(x,y,t_k) dxdy - \int_{\hat{\Omega}_{i,j}} u(x,y,t_{k-1}) dxdy. \quad (6)$$

We use a backward Euler quadrature and the divergence theorem to evaluate the second term on the left-hand side of (5)

$$\begin{aligned}\int_{t_{k-1}}^{t_k}\int_{\hat{\Omega}_{i,j}} \nabla\cdot(\vec{v}u)dxdydt &= \Delta t\int_{\hat{\Omega}_{i,j}} \nabla\cdot(\vec{v}u(x,y,t_k)dxdy + O(\Delta t^2)\\ &= \Delta t\oint_{\partial\hat{\Omega}_{i,j}} \vec{v}\cdot\vec{n}u(x,y,t_k)ds + O(\Delta t^2).\end{aligned} \tag{7}$$

Here, $\vec{n}$ denotes the unit vector normal to $\partial\hat{\Omega}_{i,j}$. We use (2) to rewrite the directional fractional derivative in a conservative form for each fixed θ

$$D_\theta\ K\ I_\theta^\beta D_\theta u = \nabla\cdot(K\ I_\theta^\beta D_\theta u\ \vec{d}_\theta), \tag{8}$$

and evaluate the dispersion term in a similar manner to (7) to arrive at

$$\begin{aligned}&-\int_{t_{k-1}}^{t_k}\int_{\hat{\Omega}_{i,j}}\Big[\int_0^{2\pi}\big(D_\theta\ K\ I_\theta^\beta D_\theta u\big)P(d\theta)\Big]dxdydt\\ &= -\Delta t\int_{\hat{\Omega}_{i,j}}\Big[\int_0^{2\pi}\big(D_\theta\ K\ I_\theta^\beta D_\theta u(x,y,t_k)\big)P(d\theta)\Big]dxdy + O(\Delta t^2)\\ &= -\Delta t\int_0^{2\pi}\Big[\int_{\hat{\Omega}_{i,j}}\big(D_\theta\ K\ I_\theta^\beta D_\theta u(x,y,t_k)\big)dxdy\Big]P(d\theta) + O(\Delta t^2)\\ &= -\Delta t\int_0^{2\pi}\Big[\oint_{\partial\hat{\Omega}_{i,j}} K\ I_\theta^\beta D_\theta u(x,y,t_k)\vec{d}_\theta\cdot\vec{n}ds\Big]P(d\theta) + O(\Delta t^2).\end{aligned} \tag{9}$$

We approximate the source and sink term as follows

$$\int_{t_{k-1}}^{t_k}\int_{\hat{\Omega}_{i,j}} f(x,y,t)dxdydt = \Delta t\int_{\hat{\Omega}_{i,j}} f(x,y,t_k)dxdy + O(\Delta t^2). \tag{10}$$

We substitute equations (6), (7), (9), and (10) into (5) and drop the local truncation error terms to obtain a control volume scheme

$$\begin{aligned}&\int_{\hat{\Omega}_{i,j}} u(x,y,t_k)dxdy + \Delta t\oint_{\partial\hat{\Omega}_{i,j}}\vec{v}\cdot\vec{n}u(x,y,t_k)ds\\ &\quad -\Delta t\int_0^{2\pi}\Big[\oint_{\partial\hat{\Omega}_{i,j}} K\ I_\theta^\beta D_\theta u(x,y,t_k)\vec{d}_\theta\cdot\vec{n}ds\Big]P(d\theta)\\ &= \int_{\hat{\Omega}_{i,j}} u(x,y,t_{k-1})dxdy + \Delta t\int_{\hat{\Omega}_{i,j}} f(x,y,t_k)dxdy.\end{aligned} \tag{11}$$

Let $\psi(\xi) := 1-|\xi|$ for $\xi \in [-1,1]$ and 0 elsewhere. Let $\{\phi_{i,j}\}_{1\le i\le N_x, 1\le j\le N_y}$ be the nodal basis functions defined by

$$\phi_{i,j}(x,y) := \psi\left(\frac{x-x_i}{h_x}\right)\psi\left(\frac{y-y_j}{h_y}\right), \qquad 1\le i\le N_x,\ 2\le j\le N_y. \tag{12}$$

Then at each time step t_k, the finite volume approximation $u_h(x,y,t_k)$ of $u(x,y,t_k)$ can be expressed as

$$u_h(x,y,t_k) = \sum_{j'=1}^{N_y}\sum_{i'=1}^{N_x} u^k_{i',j'}\phi_{i',j'}(x,y), \qquad (x,y)\in\Omega. \tag{13}$$

Let u^k and f^k be the N-dimensional vectors with $N := N_xN_y$

$$\begin{aligned} u^k &:= \left[u^k_{1,1},\dots,u^k_{N_x,1},u^k_{1,2},\dots,u^k_{N_x,2},\dots,u^k_{1,N_y},\dots,u^k_{N_x,N_y}\right]^T,\\ f^k &:= \left[f^k_{1,1},\dots,f^k_{N_x,1},f^k_{1,2},\dots,f^k_{N_x,2},\dots,f^k_{1,N_y},\dots,f^k_{N_x,N_y}\right]^T. \end{aligned} \tag{14}$$

We shall use the global indices m and n, which are related to the two-dimensional nodal indices (i,j) and (i',j') in Ω respectively by

$$\begin{aligned} m &= (j-1)N_x + i, \quad 1\le i\le N_x, \quad 1\le j\le N_y,\\ n &= (j'-1)N_x + i', \quad 1\le i'\le N_x, \quad 1\le j'\le N_y. \end{aligned} \tag{15}$$

Then f^k_m are given as

$$f^k_m := f^k_{i,j} = \int_{\hat\Omega_{i,j}} f(x,y,t_k)dxdy. \tag{16}$$

The N-by-N mass matrix $M = \left[M_{m,n}\right]_{m,n=1}^N$ and stiffness matrix $A = \left[A_{m,n}\right]_{m,n=1}^N$ are defined by

$$\begin{aligned} M_{m,n} &:= \int_{\hat\Omega_{i,j}} \phi_{i',j'}(x,y)dxdy,\\ A_{m,n} &:= -\int_0^{2\pi}\Big[\oint_{\partial\hat\Omega_{i,j}} K\ D_\theta^{-\beta}D_\theta\phi_{i',j'}\ \vec{d}_\theta\cdot\vec{n}ds\Big]P(d\theta), \end{aligned} \tag{17}$$

A key issue here is how to evaluate the advective flux $\oint_{\partial\hat\Omega_{i,j}}\vec{v}\cdot\vec{n}u(x,y,t_k)ds$ in the control volume scheme (11). A straightforward evaluation as above

will lead to a spatially symmetric discretization of the advective flux that involves the advective flux in all the four sides of the cell boundary $\partial\hat{\Omega}_{i,j}$. It is very known that the space-centered approximation to the advective term leads to nonphysical numerical oscillations [1, 10, 11, 14, 21, 24]. In contrast, upstream weighting techniques were shown to generate stable numerical approximations to advection-dominated transport equations independent of the size of mesh Peclet number [11, 21]. Hence, we adopt an upwind approximation to the advective flux flux $\oint_{\partial\hat{\Omega}_{i,j}} \vec{v}\cdot\vec{n}u(x,y,t_k)ds$, in which the approximation to the advective flux is biased in the upstream direction of the velocity field. More precisely, let B^k denote the N-by-N matrix that results from the advection term. We approximate the advective flux by the following

$$\begin{aligned}\oint_{\partial\hat{\Omega}_{i,j}} \vec{v}\cdot\vec{n}u(x,y,t_k)ds = (B^k)^{j,j}_{i,i}u^k_{i,j} + (B^k)^{j,j}_{i,i-1}u^k_{i-1,j} + (B^k)^{j,j}_{i,i+1}u^k_{i+1,j} \\ +(B^k)^{j,j-1}_{i,i}u^k_{i,j-1} + (B^k)^{j,j+1}_{i,i}u^k_{i,j+1},\end{aligned} \tag{18}$$

where

$$\begin{aligned}&(B^k)^{j,j}_{i,i} = |v_x|\Delta y + |v_y|\Delta x,\\ &(B^k)^{j,j}_{i,i-1} = -v^+_x\Delta y, \qquad (B^k)^{j,j}_{i,i+1} = v^-_x\Delta y,\\ &(B^k)^{j,j-1}_{i,i} = -v^+_y\Delta x, \qquad (B^k)^{j,j+1}_{i,i} = v^-_y\Delta x\end{aligned} \tag{19}$$

with

$$v^+_x = \max\{v_x,0\}, v^-_x = \min\{v_x,0\}, v^+_y = \max\{v_y,0\}, v^-_y = \min\{v_y,0\}. \tag{20}$$

We take the discretization in the x direction as an example. When the $v_x > 0$, the advective flux from the x direction is evaluated by $v_x(u^k_{i,j} - u^k_{i-1,j})\Delta y$. Otherwise, it is evaluated by $v_x(u^k_{i+1,j} - u^k_{i,j})\Delta y$. Then we use (15) to reformulate $(B^k)^{j,j'}_{i,i'}$ into its global $B^k_{m,n}$. It follows from (18)-(20) that each row of B^k has at most three nonzero entries. Hence, B^k is a (often strongly) nonsymmetric sparse matrix.

We substitute $u_h(x,y,t_k)$ for $u(x,y,t_k)$ in (11) to obtain an upwind control-volume scheme in a matrix form

$$\left(M + \Delta tA + \Delta tB^k\right)u^k = Mu^{k-1} + \Delta tf^k. \tag{21}$$

The upwind control volume scheme (11) is defined on a fixed mesh and is straightforward to implement. Furthermore, it is well known that an upwind scheme provides a stable numerical approximation to canonical second-order

advection-dispersion equations. However, the presence of the matrix B^k in (21) often introduces strong nonsymmetry in the discrete algebraic system, which often reduces efficiency of an iterative solver.

A major difference of the scheme (21) from its second-order analogue is that the stiffness matrix A is a full matrix. Consequently, it requires $O(N^2)$ memory. A direct solver would require $O(N^3)$ computations per time step while a Krylov subspace iterative solver would require $O(N^2)$ computations per iteration.

3. A Eulerian-Lagrangian control volume scheme

Instead of using a Eulerian space-time control volume $\hat{\Omega}_{i,j} \times [t_{k-1}, t_k]$ as in the previous section, we define a Eulerian-Lagrangian space-time prism as $R^k_{i,j}$ by extending the spatial control volume $\hat{\Omega}_{i,j}$ backward in time from t_k to t_{k-1} along the characteristics [1, 11, 24, 26]

$$\frac{dx}{dt} = v_x(x, y, t), \qquad \frac{dy}{dt} = v_y(x, y, t). \tag{22}$$

We then integrate the governing equation (1) on the Eulerian-Lagrangian space-time prism $R^k_{i,j}$ to get

$$\begin{aligned} \int_{R^k_{i,j}} \Big[\frac{\partial u}{\partial t} + \nabla \cdot (\vec{v}u) - \int_0^{2\pi} \big(D_\theta \; K \; I^\beta_\theta D_\theta u\big) P(d\theta)\Big] dxdydt \\ = \int_{R^k_{i,j}} f(x, y, t) dxdydt. \end{aligned} \tag{23}$$

Applying the divergence theorem to the first two terms on the left-hand side, we obtain

$$\begin{aligned} &\int_{R^k_{i,j}} \Big[\frac{\partial u}{\partial t} + \nabla \cdot (\vec{v}u)\Big] dxdydt \\ &= \int_{\hat{\Omega}_{i,j}} u(x, y, t_k) dxdy - \int_{\hat{\Omega}^{k-1,*}_{i,j}} u(x, y, t_{k-1}) dxdy \\ &\quad + \int_{\partial R^k_{i,j}} u[\vec{v}, 1]^T \cdot \vec{n}_{R^k_{i,j}} dS. \end{aligned} \tag{24}$$

Here $\partial R^k_{i,j}$ refers to the lateral boundary of the prism $R^k_{i,j}$, $\hat{\Omega}^{k-1,*}_{i,j}$ is the backtracked image of $\hat{\Omega}_{i,j}$ at time step t_{k-1} along the characteristics defined

by (22). Recall that a directional vector of the characteristics defined by (22) is $[\vec{v},1]^T$. That is, $[\vec{v},1]^T$ is a tangential vector of the lateral boundary $\partial R^k_{i,j}$. Hence, the last term on the right-hand side vanishes.

We utilize the Lagrangian nature of problem (1) to use the backward Euler quadrature along the characteristics to approximate the space-fractional dispersion term. We then evaluate the dispersion term at the time step t_k as in (9) to obtain

$$\begin{aligned}
&-\int_{R^k_{i,j}} \Big[\int_0^{2\pi} \big(D_\theta\ K\ I^\beta_\theta D_\theta u\big) P(d\theta)\Big] dxdydt \\
&\quad = -\Delta t \int_{\hat{\Omega}_{i,j}} \Big[\int_0^{2\pi} \big(D_\theta\ K\ I^\beta_\theta D_\theta u(x,y,t_k)\big) P(d\theta)\Big] dxdy + O(\Delta t^2) \\
&\quad = -\Delta t \int_0^{2\pi} \Big[\oint_{\partial\hat{\Omega}_{i,j}} K\ I^\beta_\theta D_\theta u(x,y,t_k) \vec{d}_\theta \cdot \vec{n} ds\Big] P(d\theta) + O(\Delta t^2).
\end{aligned} \tag{25}$$

Note that in the current context, the coefficient in the local truncation error term $O(\Delta t^2)$ involves the derivative of the unknown solution along the characteristics, instead of that in the time direction as in (9). Hence, it tends to introduce much smaller approximation error, which is an advantage of a Eulerian-Lagrangian formulation.

Substituting (24)–(25) and (10) into (23) and dropping the local truncation errors, we obtain a Eulerian-Lagrangian control-volume formulation

$$\begin{aligned}
&\int_{\hat{\Omega}_{i,j}} u(x,y,t_k) dxdy - \Delta t \int_0^{2\pi} \Big[\oint_{\partial\hat{\Omega}_{i,j}} K\ I^\beta_\theta D_\theta u\ \vec{d}_\theta \cdot \vec{n} ds\Big] P(d\theta) \\
&\quad = \int_{\hat{\Omega}^{k-1,*}_{i,j}} u(x,y,t_{k-1}) dxdy + \Delta t \int_{\hat{\Omega}_{i,j}} f(x,y,t_k) dxdy.
\end{aligned} \tag{26}$$

The Eulerian-Lagrangian formulation (26) combines the advection and accumulation terms in the governing fractional advection-dispersion equation (1) to carry out the temporal discretization in a Lagrangian coordinate. It naturally eliminates the presence of the advection term in the coefficient matrix, and so significantly reduces the nonsymmetry of the stiffness matrix for strongly advection-dominated problems that often present the most difficulties in the numerical simulation of advection-dispersion equations. The Eulerian-Lagrangian formulation (26) discretizes the space-fractional dispersion term on a fixed mesh. In fact, only the first term on the right-hand side is defined on the backtracked image $\hat{\Omega}^{k-1,*}_{i,j}$ of the control volume $\hat{\Omega}_{i,j}$. All the

other terms in (26) are defined on the fixed mesh as in the upwind control volume formulation (11). Let

$$\begin{aligned} u^{k-1,*} &:= \left[u_{1,1}^{k-1,*}, \ldots, u_{N_x,1}^{k-1,*}, u_{1,2}^{k-1,*}, \ldots, u_{N_x,2}^{k-1,*}, \ldots, u_{1,N_y}^{k-1,*}, \ldots, u_{N_x,N_y}^{k-1,*}\right]^T, \\ u_m^{k-1,*} &:= u_{i,j}^{k-1,*} = \int_{\hat{\Omega}_{i,j}^{k-1,*}} u_h(x,y,t_{k-1})dxdy, \end{aligned} \tag{27}$$

where m and i, j are related by (15). Then the Eulerian-Lagranian control-volume scheme can be formulated in the following matrix form

$$\big(M + \Delta t A\big)u^k = u^{k-1,*} + \Delta t f^k. \tag{28}$$

In the Eulerian-Lagrangian control-volume scheme (28), the mass matrix M is a well-conditioned, symmetric and positive-definite 9-banded sparse matrix. In fact, the only difference of the Eulerian-Lagrangian control-volume scheme (28) from its well-studied integer-order analogue is the presence of the space-fractional dispersion term on the fixed mesh. The Eulerian-Lagrangian control-volume scheme (28) naturally eliminates the matrix due to advection term and so greatly symmetrizes the discrete algebraic system. The price is that it has to evaluate the numerical solution on a deformed mesh at the previous time step t_{k-1}.

4. Structure of the stiffness matrix

We observe from the upwind and Eulerian-Lagrangian control volume schemes (21) and (28) that the major computational issue is an effificient storage of A and a fast matrix-vector multiplication by A. We will focus on these issues in the rest of this paper. We begin with the evaluation of the directional derivative of the trial function for any fixed direction $\theta \in [0, 2\pi)$

$$D_\theta \phi_{i',j'}(x,y) = \begin{cases} \cos\theta \dfrac{\mathrm{sgn}(x - x_{i'})}{h_x}\Big(\Big|\dfrac{y - y_{j'}}{h_y}\Big| - 1\Big) \\ + \sin\theta \dfrac{\mathrm{sgn}(y - y_{j'})}{h_y}\Big(\Big|\dfrac{x - x_{i'}}{h_x}\Big| - 1\Big), & (x,y) \in \Omega_{i',j'}, \\ 0, & (x,y) \notin \Omega_{i',j'}. \end{cases} \tag{29}$$

Subsequently, we use (3) to evaluate the fractional directional derivative. We note that

$$I_\theta^\beta D_\theta \phi_{i',j'}(x,y) = \int_{\underline{\gamma}(\theta)}^{\overline{\gamma}(\theta)} \frac{s^{\beta-1}}{\Gamma(\beta)} D_\theta \phi_{i',j'}(x - \gamma\cos\theta, x - \gamma\sin\theta)d\gamma, \tag{30}$$

where $[\underline{\gamma}(\theta), \overline{\gamma}(\theta)]$ represents the maximal interval such that $(x - \gamma\cos\theta, y - \gamma\sin\theta) \in \Omega_{i',j'}$ for all $\gamma \in [\underline{\gamma}(\theta), \overline{\gamma}(\theta)]$. Hence, the evaluation of fractional directional derivative $I_\theta^\beta D_\theta \phi_{i',j'}(x,y)$ relies on the determination of $\underline{\gamma}(\theta)$ and $\overline{\gamma}(\theta)$. To do so, we partition the domain Ω into nine subdomains that consist of the current $\Omega_{i',j'}$ and its eight neighbors as shown in Figure 1(a). We then subdivide the four corner regions into two subregions a and b by the corresponding diagonal lines. We show that in all the cases the $\underline{\gamma}(\theta)$ and $\overline{\gamma}(\theta)$ can be well determined, no matter which subdomain the point (x,y) falls into.

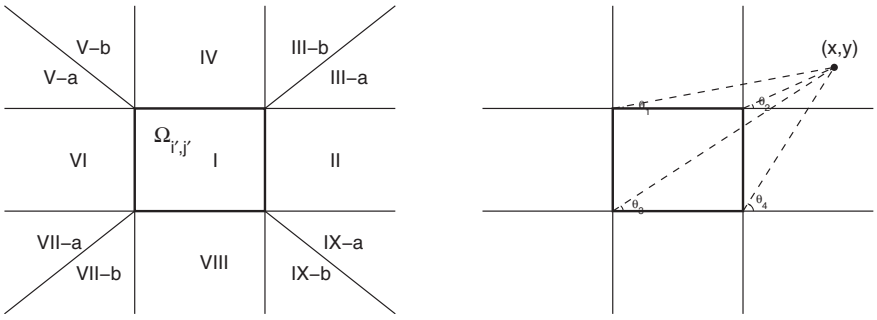

(a) Partition by means of $\Omega_{i',j'}$ (b) $(x,y) \in$ III-a

Figure 1: Illustration of partition and a representative case for determining $\underline{\gamma}(\theta)$, $\overline{\gamma}(\theta)$

We consider a representative case in Figure 1(b) that the point (x,y) falls into the upper-right corner subdomain and below the diagonal (Region III-a), and all other scenarios can be determined similarly. We connect the point (x,y) to the four vertices of $\Omega_{i',j'}$ and set the corresponding directional angles

$$\theta_1 := \arctan\frac{y - y_{j'+1}}{x - x_{i'-1}}, \qquad \theta_2 := \arctan\frac{y - y_{j'+1}}{x - x_{i'+1}},$$
$$\theta_3 := \arctan\frac{y - y_{j'-1}}{x - x_{i'-1}}, \qquad \theta_4 = \arctan\frac{y - y_{j'-1}}{x - x_{i'+1}},$$

as shown in Figure 1(b). We then set

$$\begin{aligned}
&\underline{\gamma}(\theta) := 0, && \overline{\gamma}(\theta) := 0, && \text{if } 0 \le \theta < \theta_1 \text{ or } \theta_4 \le \theta < 2\pi,\\
&\underline{\gamma}(\theta) := \frac{y - y_{j'+1}}{\sin\theta}, && \overline{\gamma}(\theta) := \frac{x - x_{i'-1}}{\cos\theta}, && \text{if } \theta_1 \le \theta < \theta_2,\\
&\underline{\gamma}(\theta) := \frac{x - x_{i'+1}}{\cos\theta}, && \overline{\gamma}(\theta) := \frac{x - x_{i'-1}}{\cos\theta}, && \text{if } \theta_2 \le \theta < \theta_3,\\
&\underline{\gamma}(\theta) := \frac{x - x_{i'+1}}{\cos\theta}, && \overline{\gamma}(\theta) := \frac{y - y_{j'-1}}{\sin\theta}, && \text{if } \theta_3 \le \theta < \theta_4.
\end{aligned}$$

We next study the structure of the stiffness matrix A.

Theorem 1. *The stiffness matrix A is a BTTB matrix.*

Proof. We express the stiffness matrix A as a N_y-by-N_y block matrix

$$A = \begin{pmatrix} A^{1,1} & A^{1,2} & \dots & A^{1,N_y} \\ A^{2,1} & A^{2,2} & \dots & A^{2,N_y} \\ \vdots & \ddots & \ddots & \vdots \\ A^{N_y,1} & A^{N_y,2} & \dots & A^{N_y,N_y} \end{pmatrix}, \tag{31}$$

with each entry $A^{j,j'}$ being an N_x-by-N_x matrix block of the form

$$A^{j,j'} = \begin{pmatrix} b^{j,j'}_{1,1} & b^{j,j'}_{1,2} & \dots & b^{j,j'}_{1,N_x} \\ b^{j,j'}_{2,1} & b^{j,j'}_{2,2} & \dots & b^{j,j'}_{2,N_x} \\ \vdots & \ddots & \ddots & \vdots \\ b^{j,j'}_{N_x,1} & b^{j,j'}_{N_x,2} & \dots & b^{j,j'}_{N_x,N_x} \end{pmatrix}. \tag{32}$$

Let the row index m and the column index n of the entry $A_{m,n}$ in the stiffness matrix A be related to (i,j) and (i',j') by (15). Here the index j corresponds to the row number of the block matrices in (31) while the index i refers to the row number in the matrix blocks in the jth row in (31). Similarly, the index j' gives the column number of the block matrices in (31) while the index i' indicates the column number in the block matrices in the j'th column in (31). Hence,

$$A_{m,n} = (A^{j,j'})_{i,i'} = b^{j,j'}_{i,i'}, \quad 1 \le i, i' \le N_x,\ 1 \le j, j' \le N_y. \tag{33}$$

To prove A is block-Toeplitz, we need to prove that for $j'_1 - j_1 = j'_2 - j_2$

$$A^{j_1,j'_1} = A^{j_2,j'_2}, \quad 1 \le j_1, j'_1, j_2, j'_2 \le N_y. \tag{34}$$

Namely, the following entrywise equalities hold

$$b_{i,i'}^{j_1,j_1'} = b_{i,i'}^{j_2,j_2'}, \qquad 1 \le i,\ i' \le N_x,\ \ 1 \le j_1, j_1', j_2, j_2' \le N_y. \tag{35}$$

Similarly, to prove that each matrix block $A^{j,j'}$ in (31) is Toeplitz, we need to prove that for $i_1' - i_1 = i_2' - i_2$

$$b_{i_1,i_1'}^{j,j'} = b_{i_2,i_2'}^{j,j'}, \quad 1 \le i_1, i_1', i_2, i_2' \le N_x, \ \ 1 \le j, j' \le N_y. \tag{36}$$

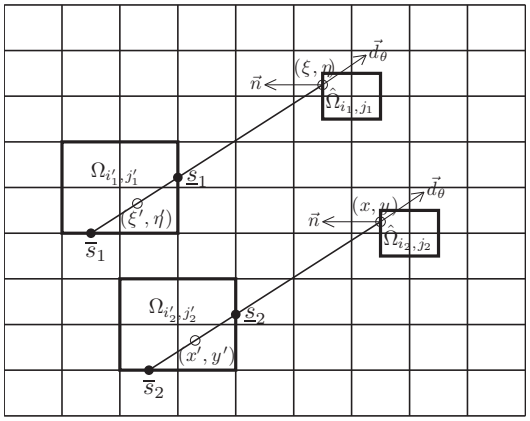

Figure 2: Illustration of the translation invariance

Let the indices (i_1, j_1), (i_1', j_1'), (i_2, j_2), and (i_2', j_2') be related by

$$i_1' - i_1 = i_2' - i_2, \qquad j_1' - j_1 = j_2' - j_2, \tag{37}$$

as in Figure 2. We prove that the following relation holds for any $\theta \in [0, 2\pi)$

$$\oint_{\partial\hat{\Omega}_{i_1,j_1}} K\ I_\theta^\beta D_\theta \phi_{i_1',j_1'}\ \vec{d}_\theta \cdot \vec{n} ds = \oint_{\partial\hat{\Omega}_{i_2,j_2}} K\ I_\theta^\beta D_\theta \phi_{i_2',j_2'}\ \vec{d}_\theta \cdot \vec{n} ds. \tag{38}$$

For any point $(x, y) \in \partial\hat{\Omega}_{i_2,j_2}$, we have either $|x - x_{i_2}| = h_x/2$ or $|y - y_{j_2}| = h_y/2$. Hence, the point (ξ, η), defined by

$$\xi := x_{i_1} + (x - x_{i_2}), \qquad \eta := y_{j_1} + (y - y_{j_2}), \tag{39}$$

satisfies either $|\xi - x_{i_1}| = h_x/2$ or $|\eta - y_{j_1}| = h_y/2$. In other words, (ξ, η) falls into $\partial\hat{\Omega}_{i_1,j_1}$. Furthermore, $\vec{n}(x, y) = \vec{n}(\xi, \eta)$.

Let $\underline{\gamma}_1(\theta)$ and $\overline{\gamma}_1(\theta)$, with $0 \le \underline{\gamma}_1(\theta) \le \overline{\gamma}_1(\theta)$, be the values of the parameter γ at which the ray extending from (ξ, η) in the direction of $-\vec{d}_\theta$ intersects $\partial\Omega_{i'_1,j'_1}$, while $\underline{\gamma}_2(\theta)$ and $\overline{\gamma}_2(\theta)$, with $0 \le \underline{\gamma}_2(\theta) \le \overline{\gamma}_2(\theta)$, be the values at which the ray extending from (x, y) in the same direction intersects $\partial\Omega_{i'_2,j'_2}$. Without loss of generality, we consider the representative case in Figure 1 to show that $\underline{\gamma}_1(\theta) = \underline{\gamma}_2(\theta)$, which we denote by $\underline{\gamma}(\theta)$, and $\overline{\gamma}_1(\theta) = \overline{\gamma}_2(\theta)$, which we denote by $\overline{\gamma}(\theta)$. As a matter of fact, we use (37) and (39) to get

$$\begin{aligned}\underline{\gamma}_1(\theta) &= \frac{\xi - x_{i'_1+1}}{\cos\theta} = \frac{(\xi - x_{i_1}) + (x_{i_1} - x_{i'_1+1})}{\cos\theta} \\ &= \frac{(x - x_{i_2}) + (x_{i_2} - x_{i'_2+1})}{\cos\theta} = \frac{(x - x_{i'_2+1})}{\cos\theta} = \underline{\gamma}_2(\theta).\end{aligned}$$

The identity $\overline{\gamma}_1(\theta) = \overline{\gamma}_2(\theta)$ can be shown in a similar way.

Next, for any $(x, y) \in \Omega_{i_2,j_2}$, the ray $x' = x - \gamma\cos\theta$, $y' = x - \gamma\sin\theta$ extending from (x, y) falls into the region $\Omega_{i'_2,j'_2}$ for $\underline{\gamma}(\theta) \le s \le \overline{\gamma}(\theta)$. Correspondingly, the ray $\xi' = \xi - \gamma\cos\theta$, $\eta' = \eta - \gamma\sin\theta$ falls into the region $\Omega_{i'_1,j'_1}$ for $\underline{\gamma}(\theta) \le \gamma \le \overline{\gamma}(\theta)$, since

$$\begin{aligned}x' - x_{i'_2} &= (x - x_{i_2}) + (x_{i_2} - x_{i'_2}) - \gamma\cos\theta \\ &= (\xi - x_{i_1}) + (x_{i_1} - x_{i'_1}) - \gamma\cos\theta = \xi' - x_{i'_1}, \\ y' - y_{j'_2} &= (y - y_{j_2}) + (y_{j_2} - y_{j'_2}) - \gamma\sin\theta \\ &= (\eta - y_{j_1}) + (y_{j_1} - y_{j'_1}) - \gamma\sin\theta = \eta' - y_{j'_1}.\end{aligned}$$

It then follows from (29) that

$$\begin{aligned}D_\theta\phi_{i'_2,j'_2}(x', y') &= \cos\theta\frac{\mathrm{sgn}(x' - x_{i'_2})}{h_x}\left(\left|\frac{y' - y_{j'_2}}{h_y}\right| - 1\right) \\ &\quad + \sin\theta\frac{\mathrm{sgn}(y' - y_{j'_2})}{h_y}\left(\left|\frac{x' - x_{i'_2}}{h_x}\right| - 1\right) \\ &= \cos\theta\frac{\mathrm{sgn}(\xi' - x_{i'_1})}{h_x}\left(\left|\frac{\eta' - y_{j'_1}}{h_y}\right| - 1\right) \\ &\quad + \sin\theta\frac{\mathrm{sgn}(\eta' - y_{j'_1})}{h_y}\left(\left|\frac{\xi' - x_{i'_1}}{h_x}\right| - 1\right) = D_\theta\phi_{i'_1,j'_1}(\xi', \eta').\end{aligned}$$

Thus,

$$\begin{aligned} I_\theta^\beta D_\theta \phi_{i'_2,j'_2}(x,y) &= \int_{\underline{\gamma}(\theta)}^{\overline{\gamma}(\theta)} \frac{\gamma^{\beta-1}}{\Gamma(\beta)} D_\theta \phi_{i'_2,j'_2}(x-\gamma\cos\theta, x-\gamma\sin\theta)d\gamma \\ &= \int_{\underline{\gamma}(\theta)}^{\overline{\gamma}(\theta)} \frac{\gamma^{\beta-1}}{\Gamma(\beta)} D_\theta \phi_{i'_2,j'_2}(x',y')d\gamma = \int_{\underline{\gamma}(\theta)}^{\overline{\gamma}(\theta)} \frac{\gamma^{\beta-1}}{\Gamma(\beta)} D_\theta \phi_{i'_1,j'_1}(\xi',\eta')d\gamma \\ &= \int_{\underline{\gamma}(\theta)}^{\overline{\gamma}(\theta)} \frac{\gamma^{\beta-1}}{\Gamma(\beta)} D_\theta \phi_{i'_1,j'_1}(\xi-\gamma\cos\theta, \eta-\gamma\sin\theta)d\gamma \\ &= I_\theta^\beta D_\theta \phi_{i'_1,j'_1}(\xi,\eta). \end{aligned}$$

We thus prove (38) and so the theorem. □

5. Fast implementation of matrix-vector multiplication

The main result in this section is the following theorem.

Theorem 2. *Both the upwind control volume scheme (21) and the Eulerian-Lagrangian control volume scheme (28) require only $O(N)$ memory. Moreover, both schemes can be carried out with a computational complexity of $O(N\log N)$ per Krylov subspace iteration per time step.*

Proof. Note that the mass matrix M and the upwind matrix B^k in the upwind scheme (21) and the mass matrix M in the Eulerian-Lagrangian scheme (28) are sparse matrices, hence they have $O(N)$ memory requirement and computational complexity per Krylov subspace iteration per time step. Hence, we need only focus on the storage and computational complexity of A.

By Theorem 1, A is BTTB. Namely, in (31) $A^{j,j'} = T_{j'-j}$ for $1 \le j, j' \le N_y$ and each T_j is Toeplitz for $1 - N_y \le j \le N_y - 1$. Hence, the stiffness matrix A can be stored in $O(N)$ memory. Moreover, each Toeplitz matrix T_j can be embedded into a $2N_x$-by-$2N_x$ circulant matrix C_j

$$C_j = \begin{pmatrix} T_j & \tilde{T}_j \\ \tilde{T}_j & T_j \end{pmatrix}$$

with $\tilde{T}_j$ determined from T_j [4]. Then the block-Toeplitz-circulant-block

(BTCB) matrix C is defined by

$$C = \begin{pmatrix} C_0 & C_1 & \dots & C_{N_y-2} & C_{N_y-1} \\ C_{-1} & C_0 & C_1 & \ddots & C_{N_y-2} \\ \vdots & \ddots & \ddots & \ddots & \vdots \\ C_{2-N_y} & \ddots & C_{-1} & C_0 & C_1 \\ C_{1-N_y} & C_{2-N_y} & \dots & C_{-1} & C_0 \end{pmatrix}.$$

Then C can be embedded into an $2N_y$-by-$2N_y$ block-circulant-circulant-block (BCCB) matrix D as follows

$$D = \begin{pmatrix} C & \tilde{C} \\ \tilde{C} & C \end{pmatrix} \tag{40}$$

with $\tilde{C}_j$ defined from C_j [4].

Let $F_{2N_y} \otimes F_{2N_x}$ be the two-dimensional discrete Fourier transform matrix. Thus, for any vector $v^{(4N)} \in \mathbb{R}^{4N}$ the matrix-vector multiplication $(F_{2N_y} \otimes F_{2N_x})v^{(4N)}$ can be carried out in $O(4N\log(4N)) = O(N\log N)$ operations via the fast Fourier transform (FFT).

Let d be the first column vector of D and

$$\hat{d} = (F_{2N_y} \otimes F_{2N_x})d. \tag{41}$$

It is known that D can be diagonalized by [4]

$$D = \big(F_{2N_y} \otimes F_{2N_x}\big)^{-1} \mathrm{diag}(\hat{d}) \big(F_{2N_y} \otimes F_{2N_x}\big). \tag{42}$$

We now prove that the matrix-vector multiplication Av for any vector $v = [v_1^T, v_2^T, \dots, v_{N_y}^T]^T \in \mathbb{R}^N$ can be carried out in $O(N\log N)$ operations. First, we expand v into $v^{(2N)} = (v_1^T, 0^T, v_2^T, 0^T, \dots, v_{N_y}^T, 0^T)^T \in \mathbb{R}^{2N}$ with each 0 being an N_x-dimensional zero vector. We further augment the vector $v^{(2N)}$ by zero vector into a vector $v^{(4N)} \in \mathbb{R}^{4N}$.

We use the fast Fourier transform to evaluate $w_1 = (F_{2N_y} \otimes F_{2N_x})v^{(4N)}$ in $O(N\log N)$ operations. Then evaluate the Hadamard product $w_2 = \hat{d} * w_1$ in $O(N)$ operations, and $w_3 = (F_{2N_y} \otimes F_{2N_x})^{-1} w_2$ in $O(N\log N)$ operations, respectively. Finally we remove the filled zero vectors to obtain a vector $w_4 \in \mathbb{R}^N$ that yields $Av = w_4$. □

The application of the fast matrix-vector multiplication algorithm to any Krylov subspace iterative solver naturally improves the computational efficiency of the solver, which reduces the computational cost from $O(N^2)$ to $O(N \log N)$ per iteration. This also reduces the round-off errors and enhances the convergence behavior of the underlying Krylov sub-space method at the same time.

6. Numerical Experiments

To examine the performance of the fast upwind control-volume scheme (21) and the Eulerian-Lagrangian control-volume scheme (28) we run several numerical experiments.

We simulate the sourceless ($f = 0$) transport of a cross which is originally centered at (0.25,0.25) and is 45° rotated from the x direction, with

Case 1: a horizontal velocity field $\vec{v} = (1, 0)$;

Case 2: a diagonal velocity field $\vec{v} = (1, 1)$.

In each case we simulate the problem with different orders of β. The maximum simulating time $T = 0.5$. In all these simulations, the probability measure $P(d\theta)$ is assumed to be atomic with atoms $\{\theta_i = i\pi/8,\ i = 0, 1, \ldots, 15\}$, i.e., the numbers of fractional derivative directions are taken 16. The advective and anomalously dispersive transport is then evaluated by the upwind control volume scheme (21) and the Eulerian-Lagrangian control-volume scheme (28). In the numerical experiments, both schemes are solved by Gaussian elimination (Gauss), the conjugate gradient squared method (CGS), and the fast conjugate gradient squared (FCGS) method. We investigate the efficiencies of these methods by comparing their consumed CPU time in solving the same equations. These methods were implemented using Intel Visual Fortran 2013 on a ThinkPad T440p Laptop.

As an example to compare the efficiencies, we list the CPU time of the three solvers for simulating Case 2 by the Eulerian-Lagrangian control-volume scheme in Table 1. The fractional derivative order is 1.5, the isotropic diffusivity coefficient $K = 0.001$. It is clearly that the FCGS solver has the highest efficiency, as shown in [25].

Next we show the variations of the cross in the advective and anomalously dispersive transport process. We simulate Case 1 and 2 by the upwind control volume scheme and the Eulerian-Lagrangian control-volume scheme and use the FCGS solver in the numerical computation. In each case, we simulate the problem with different orders of $\beta = 0.1, 0.5, 0.9$, which represent

Table 1: The consumed CPU time of the Gauss, CGS, and FCGS solvers in the numerical experiment of Case 2

	Gauss	CGS	FCGS
N_x=N_y=N_t	CPU	CPU	CPU
2^3	0.00 s	0.00 s	0.00 s
2^4	0.72 s	0.03 s	0.05 s
2^5	221.97 s	0.76 s	0.36 s
2^6	N/A	18.55 s	2.89 s
2^7	N/A	487.13 s	20.36 s
2^8	N/A	N/A	171.34 s

the different orders of fractional derivatives 1.9, 1.5, and 1.1, respectively. The isotropic diffusivity coefficient $K = 0.001$. The contours of the cross for the Eulerian-Lagrangian control-volume scheme are illustrated in Figure 3, and for the upwind control volume scheme are in Figure 4. We have the following observations:

- Figure 3 shows that the cross has very different appearances for variant values of β. It keeps its shape for $\beta = 0.9$ and diffuses gradually when β decreases, and its contours become rounded rectangles for $\beta = 0.1$. This is reasonable from the macro diffusion point of view: when β tends to 0, the anomalously dispersive transport tends to the normal second-order Fickian diffusion; when β is near 1, the anomalously dispersive transport performs more like the first-order advection. Another observation is that the contours of Case 1 and 2 are mainly the same, which shows the advantage of the Eulerian-Lagrangian control-volume scheme for remaining the physical isotropic property in different velocity fields.

- Figure 4 also shows the different appearances of the cross for variant values of β. Particularly, it cannot keep its shape for $\beta = 0.9$ due to the extra diffusivity introduced by the upwind scheme. The more serious problem is, it shows great directionality and anisotropy in the transport process for different velocity fields. The diffusion along the advective direction becomes dominative than that of the vertical direction. This non-physical anisotropic property shows the disadvantages of the upwind scheme comparing with the Eulerian-Lagrangian scheme

in dealing with the problem of advective and anomalously dispersive transport.

Finally we present examples to show the effects of anisotropic diffusive coefficients. Since the Eulerian-Lagrangian scheme is superior than the upwind scheme and the FCGS solver is the most efficient, we use them in simulating the advective and anomalously dispersive transport of the cross for both Case 1 and Case 2. In the numerical experiments, we choose anisotropic diffusive coefficients for different directions: For Case 1, let the diffusive coefficients $K_1 = 0.001$ for the directions $\theta_i, i = 6, \ldots, 12$, $K_2 = 0.01$ for the other, and vice versa. For Case 2, let the diffusive coefficients $K_1 = 0.001$ for the directions $\theta_i, i = 8, \ldots, 14$, $K_2 = 0.01$ for the other, and vice versa. Such kinds of choice can ensure the symmetry of the diffusive coefficients along the advective direction in both Case 1 and 2. The fractional order $\beta = 0.5$. The contours each cases are illustrated in Figure 5, which clearly represents the effect of anisotropic diffusivity in the transport process.

7. Conclusion

In this work we consider a time-dependent space-fractional advection-dispersion equation, which is used in modelling solute transport in groundwater. The control volume methods are proposed to numerically solve the two-dimensional problem, and the advection term is dealt with two distinct methods, the upwind and Eulerian-Lagrangian methods. The upwind schemes are easy to implement and have been widely used in practice. While, the Eulerian-Lagrangian schemes, as one of the characteristic methods, have strength in solving time-dependent advection-dispersion equations, they can provide sufficiently accurate solution with relatively fewer grids and can preserve the rotational invariance. Based on the analysis of the structure of stiffness matrix, a fast Krylov subspace iterative solver for both the upwind and Eulerian-Lagrangian control volume schemes. Several numerical experiments are provided to examine the performance of both methods. It has been shown that the Eulerian-Lagrangian control-volume scheme has the advantages for remaining the physical isotropic property in different velocity fields compared to the upwind scheme.

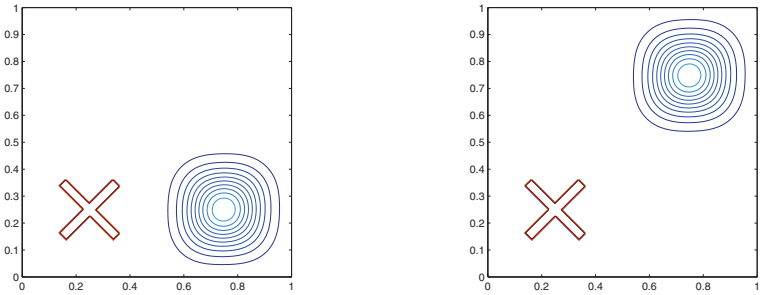

(a) Case 1: $\beta = 0.1$

(b) Case 2: $\beta = 0.1$

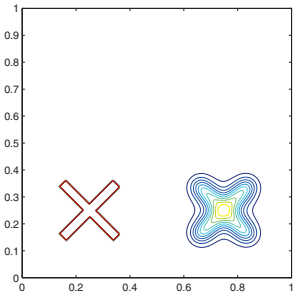

(c) Case 1: $\beta = 0.5$

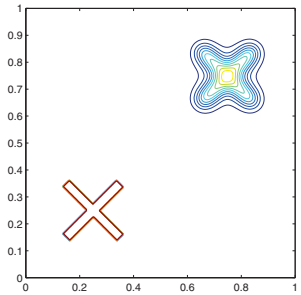

(d) Case 2: $\beta = 0.5$

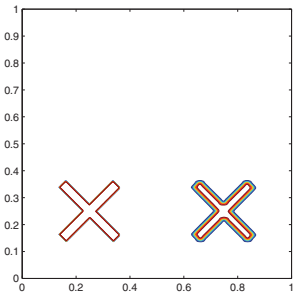

(e) Case 1: $\beta = 0.9$

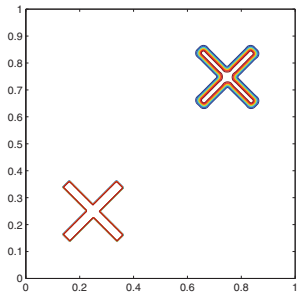

(f) Case 2: $\beta = 0.9$

Figure 3: The contours of the cross at $t = 0$ and $t = T$ solved by the Eulerian-Lagrangian control-volume scheme for Case 1, 2 with different values of β

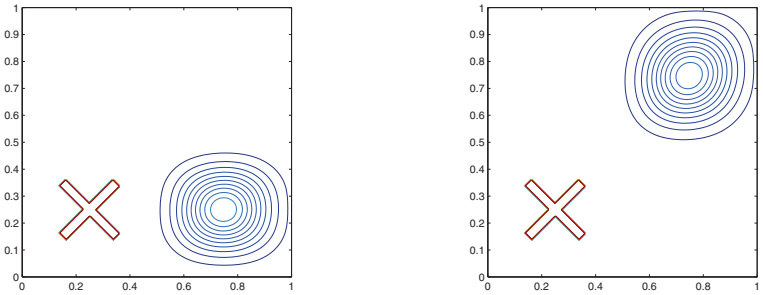

(a) Case 1: $\beta = 0.1$

(b) Case 2: $\beta = 0.1$

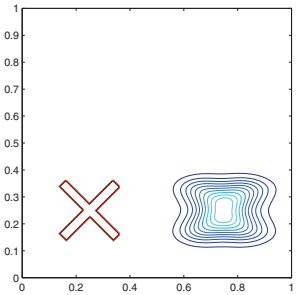

(c) Case 1: $\beta = 0.5$

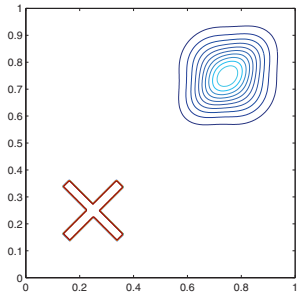

(d) Case 2: $\beta = 0.5$

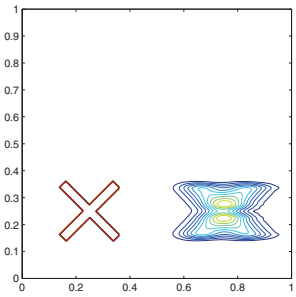

(e) Case 1: $\beta = 0.9$

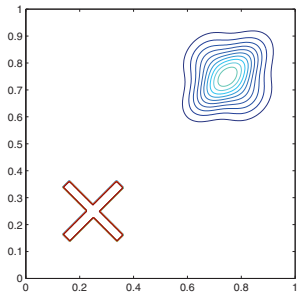

(f) Case 2: $\beta = 0.9$

Figure 4: The contours of the cross at $t = 0$ and $t = T$ solved by the upwind control-volume scheme for Case 1, 2 with different values of β

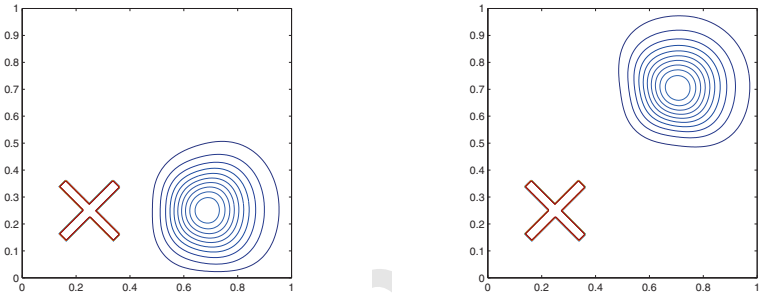

(a) Case 1: $K_1 = 0.001$, $K_2 = 0.01$ (b) Case 2: $K_1 = 0.001$, $K_2 = 0.01$

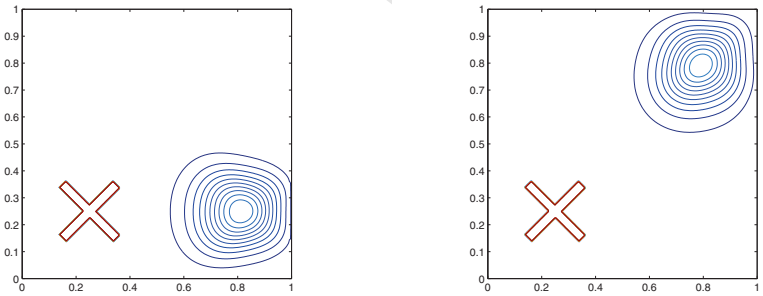

(c) Case 1: $K_1 = 0.01$, $K_2 = 0.001$ (d) Case 2: $K_1 = 0.01$, $K_2 = 0.001$

Figure 5: The contours of the cross at $t = 0$ and $t = T$ solved by the Eulerian-Lagrangian control-volume scheme for Case 1, 2 with anisotropic diffusivity

Acknowledgments

This work was funded in part by the OSD/ARO MURI Grant W911NF-15-1-0562, by the National Science Foundation under Grant DMS-1620194, by the National Natural Science Foundation of China under Grants 11971272, 11571115, 91630207, 11831010, and 11901354, and by Taishan Scholars Program of Shandong Province of China.

References

[1] T. Arbogast and M.F. Wheeler, A characteristic-mixed finite element method for advection-dominated transport problems, *SIAM Numer. Anal.*, 32 (1995), 404–424.

[2] J. Bear, *Dynamics of Fluids in Porous Materials*, Elsevier, New York, 1972.

[3] D. Benson, S.W. Wheatcraft, and M.M. Meerschaert, The fractional-order governing equation of Lévy motion, *Water Resour. Res.*, 36 (2000), 1413–1423.

[4] R.H. Chan and M.K. Ng, Conjugate gradient methods for Toeplitz systems, *SIAM Review*, 38 (1996), 427–482.

[5] A. Cheng, H. Wang, and K. Wang, A Eulerian-Lagrangian control volume method for solute transport with anomalous diffusion, *Numer Methods Partial Diff Eqns* 31 (2015), 253–267.

[6] N. Du and H. Wang, A fast finite element method for space-fractional dispersion equations on bounded domains in $\mathbb{R}^2$, *SIAM J. Sci. Comput.*, 37 (2015), A1614–A1635.

[7] V.J. Ervin, N. Heuer, J.P. Roop, Numerical approximation of a time dependent, nonlinear, space-fractional diffusion equation, *SIAM J. Numer. Anal.*, 45 (2007), 572–591.

[8] V.J. Ervin and J.P. Roop, Variational solution of fractional advection dispersion equations on bounded domains in $\mathbb{R}^d$, *Numer. Methods. Partial Differential Eq.*, 23 (2007), 256–281.

[9] R.E. Ewing (Ed.). The Mathematics of Reservoir Simulation. Research Frontiers in Applied Mathematics 1, SIAM, Philadelphia, 1984.

[10] R.E. Ewing, T.F. Russell, and M.F. Wheeler, Convergence analysis of an approximation of miscible displacement in porous media by mixed finite elements and a modified method of characteristics, *Comput. Methods Appl. Mech. Engrg.*, 47 (1984), 73–92.

[11] R.E. Ewing and H. Wang, A summary of numerical methods for time-dependent advection-dominated partial differential equations, David Sloan, Endre Suli, and Stefan Vandewalle, (eds.), *Numer Anal 2000 in the 20th Century* 7, *J Comput Appl Math* 128 (2001), 423–445.

[12] X. Guo, Y. Li, and H. Wang, A fourth-order scheme for space fractional diffusion equations, *J. Comput. Phys.*, 737 (2018), 410–424.

[13] J. Jia and H. Wang, A Fast Finite Volume Method on Locally Refined Meshes for Fractional Diffusion Equations, *East. Asia. J. Appl. Math.*, 9 (2019), 755–779.

[14] R.J. LeVeque, *Finite volume methods for hyperbolic problems*, Cambridge Texts in Applied Mathematics, Cambridge University Press, Cambridge, 2002.

[15] F. Liu, V. Anh, and I. Turner, Numerical solution of the space fractional Fokker-Planck equation, *J. Comput. Appl. Math.*, 166 (2004), 209–219.

[16] M.M. Meerschaert, D.A. Benson, and B. Baeumer, Multidimensional advection and fractional dispersion, *Phys. Rev. E*, 59 (1999), 5026–5028.

[17] M.M. Meerschaert, H.P. Scheffler, and C. Tadjeran, Finite difference methods for two-dimensional fractional dispersion equation, *J. Comput. Phys.*, 211 (2006), 249–261.

[18] M.M. Meerschaert and A. Sikorskii, *Stochastic Models for Fractional Calculus*, De Gruyter Studies in Mathematics, 2011.

[19] R. Metzler and J. Klafter, The restaurant at the end of the random walk: recent developments in the description of anomalous transport by fractional dynamics, *J. Phys. A Math. Gen.*, 37 (2004), R161-R208.

[20] J.P. Roop, Computational aspects of FEM approximation of fractional advection dispersion equations on bounded domains in $\mathbb{R}^2$, *J. Comput. Appl. Math.*, 193 (2006), 243–268.

[21] H.-G. Roos, M. Stynes, and L. Tobiska, *Robust Numerical Methods for Singularly Perturbed Differential Equations*, 2nd edition, Springer Series in Computational Mathematics Volume 24, Springer-Verlag, Berlin, 2008.

[22] H. Wang and M. Al-Lawatia, A locally conservative Eulerian-Lagrangian control-volume method for transient advection-diffusion equations, *Numer Methods Partial Diff Eqns* 22 (2005) 577-599.

[23] H. Wang and T.S. Basu, A fast finite difference method for two-dimensional space-fractional diffusion equations, *SIAM J. Sci. Comput.*, 34 (2012), A2444–A2458.

[24] H. Wang, H.K. Dahle, R.E. Ewing, M.S. Espedal, R.C. Sharpley, and S. Man, An ELLAM Scheme for advection-diffusion equations in two dimensions, *SIAM J. Sci. Comput.*, 20, (1999) 2160–2194.

[25] H. Wang and N. Du, A fast finite difference method for three-dimensional time-dependent space-fractional diffusion equations and its efficient implementation, *J. Comput. Phys.*, 253 (2013), 50–63.

[26] H. Wang, R.E. Ewing, G. Qin, S.L. Lyons, M. Al-Lawatia, and S. Man, A family of Eulerian-Lagrangian localized adjoint methods for multi-dimensional advection-reaction equations, *J Comput Phys* 152 (1999) 120–163.

[27] H. Wang, D. Liang, R.E. Ewing, S.L. Lyons, and G. Qin, An approximation to miscible fluid flows in porous media with point sources and sinks by an Eulerian-Lagrangian localized adjoint method and mixed finite element methods, *SIAM J Sci Comput* 22 (2000), 561–581.

[28] H. Wang, D. Liang, R.E. Ewing, S.L. Lyons, and G. Qin, An ELLAM-MFEM solution technique for compressible fluid flows in porous media with point sources and sinks, *J Comput Phys* 159 (2000), 344–376.

[29] H. Wang, K. Wang, and T. Sircar, A direct $O(N \log^2 N)$ finite difference method for fractional diffusion equations, *J. Comput. Phys.*, 229 (2010), 8095–8104.

[30] K. Wang and H. Wang, A fast characteristic finite difference method for fractional advection-diffusion equations, *Adv. Water Resour.*, 34 (2011), 810–816.

[31] S. Wu, H. Zhang, and T. Zhou, Solving time periodic fractional diffusion equations via diagonalization technique and multigrid, *Numer. Linear Algebra Appl.*, 25 (2018), e2178.

[32] S. Wu and T. Zhou, Fast parareal iterations for fractional diffusion equations, *J. Comput. Phys.*, 329 (2017), 210–226.

[33] Y. Zhang, D.A. Benson, M.M. Meerschaert, and E.M. LaBolle, Space-fractional advection-dispersion equations with variable parameters: Diverse formulas, numerical solutions, and application to the MADE-site data, *Water Resour. Res.*, 43 (2007), W05439.

Declaration of interests

☒ The authors declare that they have no known competing financial interests or personal relationships that could have appeared to influence the work reported in this paper.

☐The authors declare the following financial interests/personal relationships which may be considered as potential competing interests: